Theory of the BOLD Effect in the Capillary Region: An Analytical Approach for the Determination of T_2^* in the Capillary Network of Myocardium

Wolfgang R. Bauer,[1]* Walter Nadler,[2] Michael Bock,[3] Lothar R. Schad,[3] Christian Wacker,[2] Andreas Hartlep,[3] and Georg Ertl[1]

This article presents an analytical approach for the quantification of the blood oxygen level dependent (BOLD) effect in the capillary region. The capillary geometry of myocardium is considered. The relaxation rate R_2^* is determined as a function of the capillary radius R_c, the intracapillary volume fraction RBV, and the diffusion coefficient D. When the intracapillary volume fraction is small, the approximation $R_2^* = \text{RBV} \cdot \tau^{-1} \cdot (\sqrt{1 + (\tau\delta\omega)^2} - 1)$ is valid, with the correlation time $\tau = (R_c^2/4D) \cdot (|\ln \text{RBV}|/(1 - \text{RBV}))$. The predictions of this model agree well with numerical simulations and experimental data of others and with data recently measured by our group. **Magn Reson Med 41:51–62, 1999.** © 1999 Wiley-Liss, Inc.

Key words: BOLD effect; capillary; myocardium; transverse relaxation

INTRODUCTION

The BOLD (blood oxygen level dependent) effect in tissue results from the paramagnetic deoxyhemoglobin in capillaries and venous vessels. In addition to its application in functional imaging of the brain (1), the BOLD effect has been observed in cardiac imaging (2–5). This application bears a great potential for the diagnosis of ischemic heart disease. However, a quantitative model that considers parameters of myocardial microcirculation is a prerequisite. Although it is not a problem to understand the BOLD effect qualitatively, its quantitative analysis is very complex and demands further evaluation. The acceleration of the transverse relaxation depends on the concentration of deoxyhemoglobin in the vessels and the geometry of the vessel network. Yablonski and Haake (6) studied some geometries of cylindrical vessels filled with a (para)magnetic substance and determined the dephasing of spins induced by the inhomogeneous magnetic field in such vessel networks. In their work, the authors considered the spins as stationary (static dephasing regime), i.e., the diffusion of spins during relaxation was neglected. This approximation is justified as long as the amplitude of the field fluctuations that a diffusing nuclear spin "sees" during relaxation is much smaller than the magnitude of this inhomogeneous field.

This theory, however, does not describe the BOLD effect in myocardium, at least when clinical imaging systems (<2 T) are used, for the following reason: concerning the myocardial blood volume, the dominating vessels are the capillaries with a volume fraction of more than 90% of the intramyocardial blood volume (7). The capillaries are arranged parallel with an intercapillary distance of about 19 μm, i.e., one can assume a kind of periodicity of the BOLD-related inhomogeneous field after this distance. Typical relaxation times of transverse magnetization in these low-field systems are in the range of $T_2^* = 30$–40 ms. Thus, the diffusion distance during relaxation ($t > 2 \times T_2^*$) is $\sqrt{tD} > 7$ μm (diffusion coefficient $D = 1$ μm²/ms), i.e., taking into account the intercapillary distance a nuclear spin "sees" nearly the whole variation of the inhomogeneous field. Hence, the field fluctuations due to diffusion are in the range of the magnitude of the inhomogeneous field, which excludes the application of the theory of Yablonski and Haake.

Another analytical approach to determine transverse relaxation exists as long as the *motional narrowing* condition is valid. This condition states that the product of correlation time and the magnitude of the field fluctuations has to be significantly smaller than 1. When this condition is fulfilled, the relaxation rate is simply

$$R_2^* = \tau \cdot \langle\omega^2\rangle$$

where τ is the correlation time and $\langle\omega^2\rangle$ the variance of the precession frequency of the inhomogeneous field. Although this approach can be widely used in other fields (8), it is not appropriate for the description of the BOLD effect in the capillary system. A crude approximation that provides the magnitude of the correlation time is given by the diffusion time $\tau = R_c^2/D$, where $R_c \approx 2.5$ μm and is the capillary radius and $D = 1$ μm²/ms and is the diffusion constant. The equatorial field around a capillary in a low-field system (e.g., 1.25 T) may be estimated to be in the range of 1 mgauss, i.e., the frequency is $\delta\omega = 168$ rad s^{-1} (6). Hence, the product $\tau \cdot \delta\omega \approx 1$ does not fulfill the motional narrowing condition.

Since there is no sufficient theory of the BOLD effect in the capillary region, and since in at least some tissues such as myocardium the capillary fraction clearly dominates, our intention was to develop an analytical approach to determine the transverse relaxation rate as a function of the capillary/tissue geometry and the intracapillary BOLD-related magnetization. In this study, we will only focus on the decay of the transverse magnetization, which, for example, can be observed in gradient echo sequences, i.e.

this decay is due to reversible and irreversible dephasing of transverse polarized spins. The article is structured as follows: we will first construct a model of the capillary system and tissue that reflects the geometry and topology in myocardium. In the mathematical analysis, we will first derive an expression of the correlation time of field fluctuations that nuclear spins are subjected to while diffusing in our tissue model. Thereafter, we will demonstrate that we can replace the exact time evolution of transverse magnetization determined by the Bloch-Torrey equation (9) by a *strong collision* approximation. In contrast to other approaches, e.g., the *motional narrowing* approximation, the *strong collision* approximation is not based on any assumption of the relation of local field strength and correlation time. Instead, its application is justified when the local field fluctuations are rapid when compared with relaxation. The *strong collision* approximation leads directly to an analytical expression of the Laplace transform of the relaxation process, and this transform will provide the relaxation time. In the following section, we will compare our results with the computer simulations of Kennan et al. (10) and the experimental data of Atalay et al. (2, 3) and our own group (C. Wacker, et al., Noninvasive assessment of myocardial oxygenation and perfusion without exogenous contrast agents using T_2^* and T_1, manuscript submitted).

TISSUE MODEL

1. The BOLD effect in tissue arises from the paramagnetic property of deoxyhemoglobin, which, confined in capillaries and venous vessels, induces a perivascular inhomogeneous magnetic field in the presence of an external magnetic field. The blood volume fraction of capillaries in myocardium is more than 90% of the whole myocardial blood volume (arterial plus capillary plus venous compartment) (7), i.e., the fraction of the venous compartment is less than 10%. This finding implies that in myocardium the volume contribution of the capillaries to the BOLD effect is clearly dominating. In our model, therefore, we will consider only this vessel type.

2. The BOLD-related transverse relaxation of spins is induced by the inhomogeneous magnetic field around vessels containing deoxyhemoglobin. Since oxygen delivery from blood to tissue takes place in capillaries, there is a gradient of deoxyhemoglobin along the capillary axis, i.e., there is also a pericapillary magnetic field gradient in this direction. In myocardium, capillaries are arranged in parallel to the muscle fibers. The intercapillary distance is ≈ 19 μm (11) and the length of a single capillary is more than 400 μm (11). Since the diffusion coefficient of water is about $D = 1$ μm²/ms and typical values for T_2^* in myocardium are in the range of 35 ms, the range of the diffusion distance along the capillary axis within relaxation ($t \approx 2 - 3 \times T_2^*$) is $\sqrt{tD} \approx 8$–10 μm, i.e., the diffusion distance is short compared with the capillary length. Due to the length of the capillary and this short diffusion distance, the contribution of diffusion in the direction of the capillary axis to relaxation is negligible when compared with that of perpendicular diffusion. Hence, we only consider diffusion of spins in the cross-sectional plane of the capillary bed.

3. We only consider two compartments in tissue: the intracapillary volume plus the capillary wall and the extracapillary tissue. Since the interstitial-intracapillary exchange rate of water protons was found to be less than 7 Hz (12), the extracapillary to intracapillary transport rate is small compared with the relaxation rate T_2^{*-1} and, therefore, is neglected. In our model, we assume, therefore, reflectory boundary conditions at the capillary wall for a diffusing nuclear spin of the interstitial space. Furthermore, we only consider the extracapillary fraction of nuclear spins, due to their dominating contribution (>90%) to overall magnetization.

4. In myocardium, the capillaries and muscle fibers form an almost regular structure. Therefore, it is reasonable to assign each capillary an area of tissue that is predominantly supplied by this capillary. According to Krogh's capillary model, this supply area is a coaxial cylinder around the capillary the radius of which is $R_s = 1/\sqrt{\pi \times \text{capillary density}}$. In our mathematical model, we restrict diffusion of spins to this area. The legitimization for this restriction and its mathematical implications for evaluation of diffusion have already been discussed in detail (13). One implication is that reflectory diffusive boundary conditions have to be assumed for the trajectories of a nuclear spin at R_s, i.e., trajectories of spins that pass from the supply area of the capillary under observation to that of the neighboring capillary are replaced by symmetric trajectories that are located within the original supply area. Together with Paragraphs 2 and 3, this implies that the diffusion space is the area between concentric circles: the inner one with the capillary radius R_c, the outer one with the supply radius R_s (Fig. 1). Within this diffusion space, we only consider the interaction of a nuclear spin with the magnetic field around the central capillary, which
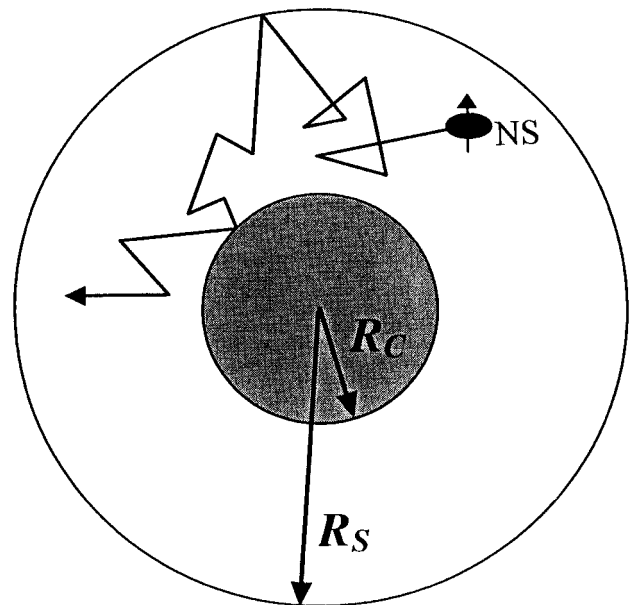
FIG. 1. Cross-sectional view of the capillary plus the coaxial surrounding supply tissue with the trajectory of a diffusing nuclear spin (NS) according to our model (see text). The radius of the capillary is denoted as R_c that of the supply area as R_s. Reflectory diffusive boundary conditions are assumed at the outer capillary wall and the periphery of the supply area.

is generated by the paramagnetic deoxyhemoglobin. According to basic magnetostatics (e.g., ref. 14) the difference of intracapillary to extracapillary magnetization in the presence of an external magnetic field B_0 is determined by (cgs units)

$$\Delta M = \Delta\chi \cdot B_0 \cdot \sin^2(\theta) \tag{1}$$

with $\Delta\chi$ as the difference of the volume susceptibility (e.g., $\Delta\chi = 8 \cdot 10^{-8}$ for deoxygenated blood with a hematocrit of 40% (6, 10)) and the tilt angle θ between the capillary axis and the direction of the external field. The Larmor frequency around the capillary is then determined by (14)

$$\omega(r, \phi) = -\delta\omega \cdot R_c^2 \cos(2\phi)/r^2 \tag{2}$$

with the cylindrical coordinates $x = (r, \phi)$ in the cross-sectional plane of the capillary. The term $\delta\omega$ is the characteristic equatorial shift of the radial frequency of a magnetized cylinder, i.e., $\delta\omega = |\omega(R_c, 0)|$, which according to magnetostatics is

$$\delta\omega = 2\pi\gamma \cdot \Delta M \tag{3}$$

with γ as the gyromagnetic ratio.

MATHEMATIC ANALYSIS

Determination of the Correlation Time

When we consider the trajectories $x_j(t)$ of an ensemble of N spins, the autocorrelation function $K(t)$ of the local NMR frequencies $\omega(x)$ is determined by (We assume that the spatial average of $\omega(x)$ vanishes, which is valid for our model (see Eq. [2]). In general, this outcome can always be achieved by normalization of $\omega(x)$.)

$$K(t) = \frac{1}{N}\sum_{j=1}^{N} \omega(x_j(t)) \cdot \omega(x_j(0)) \tag{4}$$

or when $p(x, x_0, t)$ defines the probability density to find a spin at the point x after the time t with the initial ($t = 0$) position x_0

$$K(t) = \int_V dx \int_V dx_0\, \omega(x) \cdot p(x, x_0, t) \cdot \omega(x_0) \cdot p(x_0) \tag{5}$$

where $\int_V$ denotes the integration over the diffusion space with volume V, and $p(x_0)$ defines the probability density function of the steady state, i.e., in this case, it is identical with the spin density, which may be assumed to be homogeneous in tissue, $p(x_0) = 1/V$. Since we assume free diffusion of spins within the boundaries $R_c \leq |x| \leq R_s$, the probability $p(x, x_0, t)$ is simply the Green's function of the diffusion equation

$$\partial_t p(x, x_0, t) = D\nabla^2 p(x, x_0, t) \tag{6}$$

i.e.,

$$p(x, x_0, t) = \exp(D\nabla^2 \cdot t)\delta(x - x_0) \tag{7}$$

with the reflectory boundary conditions $\partial_r p(x, x_0, t) = 0$ for $|x| = R_c, R_s$. In general, the function $K(t)$ may be quite complicated; however, usually a single exponential decay is assumed, i.e.,

$$K(t) = K(0) \cdot \exp(-t/\tau) \tag{8}$$

where τ is the correlation time. The correlation time provides an information on the time after which the fluctuations of the local fields may be considered as stochastically independent, i.e., when $t \geq 2\tau$ the probability density $p(x, x_0, t)$ satisfies the relation

$$p(x, x_0, t) \approx p(x) \tag{9}$$

One way to approximate the correlation function by a single exponential function is given by the *mean relaxation* time approximation (15)

$$\tau = \int_0^\infty dt\, K(t)/K(0) \tag{10}$$

and with Eqs. [5] and [7] (see Appendix).

$$\tau = \frac{1}{K(0) \cdot D \cdot V} \int_V dx\, \omega(x) \left[-\frac{1}{\nabla^2}\right]\omega(x)$$

$$= \frac{1}{2D} \cdot \frac{\ln(R_s/R_c)}{R_c^{-2} - R_s^{-2}} = -\frac{R_c^2}{4D} \cdot \frac{\ln(\text{RBV})}{1 - \text{RBV}} \tag{11}$$

where $\text{RBV} = R_c^2/R_s^2$ is the volume fraction of capillary space (regional blood volume).

Time Evolution of the Magnetization

In this section, we will demonstrate the most important step in the development of our model. We will replace the exact time evolution of the magnetization by an evolution based on the *strong collision* approach. The term *strong collision* derives from the original field of application of this approximation in statistical physics. When we consider diffusion of spins within an inhomogeneous magnetic field, the time evolution of the local transverse magnetization (notation in polar form, i.e., $m = m_x - im_y$) is determined by the Bloch-Torrey (9) equation

$$\partial_t m(x, t) = (D\nabla^2 + i \cdot \omega(x))m(x, t) \tag{12}$$

which, after formal time integration, provides

$$m(x, t) = \exp[(D\nabla^2 + i \cdot \omega(x)) \cdot t]m(x, 0) \tag{13}$$

and for the whole magnetization

$$M(t) = \frac{1}{V}\int_V dx \exp[(D\nabla^2 + i \cdot \omega(x)) \cdot t]m(x, 0) \tag{14}$$

where $\omega(x)$ is the local precession frequency. There are only a few cases in which Eqs. [12]–[14] can be solved analytically, e.g., when $\omega(x)$ is the frequency of a linear gradient field. In general, however, only numerical calculations or computer simulations (10) may be applied to determine the time course of transverse magnetization.

When we determine the correlation time of the local field fluctuations that influence a diffusing nuclear spin, we obtain for typical values of myocardium (RBV = 5–10%, $R_c = 2.75$ μm, $D = 1$ μm²/ms) $\tau \leq 6$ ms. Typical relaxation times of the transverse magnetization in myocardium are in the range of $T_2^* = 30$–40 ms for magnets used in clinical imaging systems. Since T_2^* describes the influence of both, non-BOLD and BOLD effects on relaxation, a relaxation time describing only the BOLD effects would be even longer. Hence, the time scale on which the local fields are correlated is much smaller than the time scale of the relaxation related to the BOLD effect. This finding implies that, on the time scale of this transverse relaxation, the local fields are uncorrelated.

Strong Collision Approximation

We, therefore, make the approximation to replace the diffusion operator $D\nabla^2$ in Eqs. [12]–[14] by an operator

$$\mathbf{D} = \lambda(\mathbf{II} - \mathbf{id}) \qquad [15]$$

(16, 17) where $\mathbf{II}$ denotes the projection operator onto the functional space generated by the steady state probability function $p(x)$, i.e., the application of this operator on a function $f(x)$ is

$$\mathbf{II}f(x) = p(x) \cdot \int_V dx\, f(x) \qquad [16]$$

and $\mathbf{id}$ is the identity, i.e.,

$$\mathbf{id}\, f(x) = f(x) \qquad [17]$$

The operator $\mathbf{D}$ describes the stochastic field fluctuations as a stationary Markov process with the transition rates between two distinct local field realizations $\omega(x)$, $\omega(x_0)$ as $\lambda \cdot p(x)$, i.e., the rate is independent of the initial state. An approach of this type is referred to as *random phase* or *strong collision* approximation (16, 17). Since in myocardium the water proton density is rather homogeneous, the probability density function of the steady state is simply $p(x) = 1/V$.

The Green's function $p_D(x, x_0, t)$ of this transition operator $\mathbf{D}$ is

$p_D(x, x_0, t) = \exp(\mathbf{D} \cdot t)\delta(x - x_0)$

$\qquad = \exp(-\lambda t(\mathbf{id} - \mathbf{II}))\delta(x - x_0)$

$\qquad = \displaystyle\sum_{\nu=0}^{\infty} \frac{(-\lambda t)^\nu}{\nu!} (\mathbf{id} - \mathbf{II})^\nu\, \delta(x - x_0)$

$\qquad = \left[\mathbf{id} + \displaystyle\sum_{\nu=1}^{\infty} \frac{(-\lambda t)^\nu}{\nu!} (\mathbf{id} - \mathbf{II})\right] \delta(x - x_0)$

$\qquad = \left[\mathbf{II} + \mathbf{id} - \mathbf{II} + \displaystyle\sum_{\nu=1}^{\infty} \frac{(-\lambda t)^\nu}{\nu!} (\mathbf{id} - \mathbf{II})\right] \cdot \delta(x - x_0)$

$\qquad = [\mathbf{II} + e^{-\lambda t}(\mathbf{id} - \mathbf{II})]\delta(x - x_0)$

$\qquad = p(x) \cdot (1 - e^{-\lambda t}) + e^{-\lambda t}\delta(x - x_0) \qquad [18]$

where we applied the idempotency of the projection operator $(\mathbf{id} - \mathbf{II})$, i.e., $(\mathbf{id} - \mathbf{II})^\nu = (\mathbf{id} - \mathbf{II})$ for $\nu \geq 1$. The transition rate λ in the *strong collision* operator [15] is determined self consistently. We require that $\mathbf{D}$ reproduces the correlation time τ of the local field fluctuations (Eq. [11]). Since the correlation function of the field fluctuations determined by the *strong collision* Green's function p_D (Eqs. [5] and [18]) is

$$K_D(t) = \int_V dx \int_V dx_0\, \omega(x) \cdot p_D(x, x_0, t) \cdot \omega(x_0) \cdot p(x_0)$$

$$= K_D(0) \cdot e^{-\lambda t} \qquad [19]$$

the transition rate has to be set as

$$\lambda = \frac{1}{\tau} \qquad [20]$$

The Eqs. [18] and [20] demonstrate that on the time scale of the evolution of magnetization ($\gg\tau$) the relation

$$p_D(x, x_0, t) \approx p(x) \qquad [21]$$

holds. Comparison with Eq. [9] shows that, in this case, the Green's function of the exact diffusion process $p(x, x_0, t)$ is equivalent to the Green's function of the stochastical process determined by the operator $\mathbf{D}$ (Eq. [15]). Therefore, it is justified to rewrite Eqs. [13] and [14] as

$$m(x, t) = \exp\left[(\mathbf{D} + i \cdot \omega(x)) \cdot t\right]m(x, 0) \qquad [22]$$

or for the whole magnetization

$$M(t) = \frac{1}{V}\int_V dx\, \exp\left[(\mathbf{D} + i \cdot \omega(x)) \cdot t\right]m(x, 0) \qquad [23]$$

Determination of Relaxation Time

Instead of solving Eq. [23], it is more suitable to consider the Laplace transform of the magnetization decay, i.e.,

$$\hat{M}(s) = \int_0^\infty dt\, e^{-s \cdot t} \cdot M(t) \qquad [24]$$

$$= \frac{1}{V}\int_V dx\, \frac{1}{s - \mathbf{D} - i \cdot \omega(x)}\, m(x, 0) \qquad [25]$$

$$= \frac{1}{V}\int_V dx\, \frac{1}{s - \tau^{-1}(\mathbf{II} - \mathbf{id}) - i \cdot \omega(x)} \qquad [26]$$

where we assume homogeneity of the initial magnetization, which had been normalized to $m(x, 0) = 1$.

It is useful to decompose $s - \mathbf{D} - i \cdot \omega(x)$ into (see Eqs. [15] and [16]) $A = (s + \tau^{-1})\mathbf{id} - i \cdot \omega(x)$ and $B = -\tau^{-1}\mathbf{II} = -\tau^{-1} \cdot V^{-1}\int_V dx$ and to transform Eq. [26] according to the

operator identity $1/(A + B) = 1/A - (1/A) \cdot B \cdot 1/(A + B)$, i.e.,

$$\hat{M}(s) = \underbrace{\frac{1}{V} \int_V dx \frac{1}{(s + \tau^{-1})\mathbf{id} - i \cdot \omega(x)}}_{= \hat{M}_0(s + \tau^{-1})}$$

$$+ \underbrace{\frac{1}{V} \int_V dx \frac{1}{(s + \tau^{-1})\mathbf{id} - i \cdot \omega(x)}}_{= \hat{M}_0(s + \tau^{-1})}$$

$$\cdot \tau^{-1} \cdot \underbrace{\frac{1}{V} \int_V dx \frac{1}{s - \mathbf{D} - i \cdot \omega(x)}}_{= \hat{M}(s)}$$

$$= \hat{M}_0(s + \tau^{-1}) + \tau^{-1}\hat{M}_0(s + \tau^{-1}) \cdot \hat{M}(s) \qquad [27]$$

where $\hat{M}_0(s)$ is the Laplace transform of the time course of magnetization that would be present in the absence of diffusion (static dephasing regime). Equation [27] straightforwardly gives the expression of the Laplace transform $\hat{M}(s)$

$$\hat{M}(s) = \frac{\hat{M}_0(s + \tau^{-1})}{1 - \tau^{-1} \cdot \hat{M}_0(s + \tau^{-1})} \qquad [28]$$

When the local frequency around the capillary is given by Eq. [2], $\hat{M}_0(s)$ has the form (see Appendix)

$$\hat{M}_0(s) = \frac{R_c^2 + R_s^2}{\sqrt{s^2 R_s^4 + \delta\omega^2 R_c^4} + R_c^2 \sqrt{s^2 + \delta\omega^2}} \qquad [29]$$

and, hence,

$$\hat{M}(s) = (R_c^2 + R_s^2) \cdot \left(\sqrt{(s + \tau^{-1})^2 R_s^4 + \delta\omega^2 R_c^4} \right.$$

$$\left. + R_c^2 \sqrt{(s + \tau^{-1})^2 + \delta\omega^2} - \tau^{-1}(R_c^2 + R_s^2) \right)^{-1}$$

$$= (1 + RBV) \cdot \left(\sqrt{(s + \tau^{-1})^2 + \delta\omega^2 RBV^2} \right.$$

$$\left. + RBV \sqrt{(s + \tau^{-1})^2 + \delta\omega^2} - \tau^{-1}(1 + RBV) \right)^{-1} \qquad [30]$$

In principle, the Laplace transform $\hat{M}(s)$ provides all information about the relaxation of magnetization. The time course could be obtained by backward transformation; however, this process is very cumbersome. We are interested in the relaxation time T_2^*, i.e., the time constant that approximates best the magnetization decay by a single exponential function

$$M(t) = e^{-t/T_2^*} \qquad [31]$$

This relaxation time can be determined according to the *mean relaxation time approximation* (15) as

$$T_2^* = \int_0^\infty dt \, M(t) \qquad [32]$$

A comparison with Eq. [24] shows that

$$T_2^* = \hat{M}(0) \qquad [33]$$

i.e., according to Eq. [30]

$$T_2^* = (1 + RBV) \cdot \left(\sqrt{\tau^{-2} + \delta\omega^2 RBV^2} \right.$$

$$\left. + RBV \cdot \sqrt{\tau^{-2} + \delta\omega^2} - \tau^{-1}(1 + RBV) \right)^{-1}$$

$$= \tau \cdot (1 + RBV) \cdot \left(\left[\sqrt{1 + (\tau\delta\omega \cdot RBV)^2} - 1 \right] \right.$$

$$\left. + RBV \cdot \left[\sqrt{1 + (\tau\delta\omega)^2} - 1 \right] \right)^{-1}, \qquad [34]$$

or when considering the rate $R_2^* = 1/T_2^*$,

$$R_2^* = \tau^{-1} \cdot \frac{1}{1 + RBV} \cdot \left(\left[\sqrt{1 + (\tau\delta\omega \cdot RBV)^2} - 1 \right] \right.$$

$$\left. + RBV \cdot \left[\sqrt{1 + (\tau\delta\omega)^2} - 1 \right] \right) \qquad [35]$$

APPLICATIONS

Approximations

Although Eq. [35] may appear rather complex, it can, however, be transformed to a more suitable form for certain limiting cases.

Motional Narrowing Limit

In the motional narrowing limit ($\tau \cdot \delta\omega \ll 1$) one obtains for the relaxation rate from Eq. [35]

$$R_2^* = \tau \cdot \left(RBV \cdot \frac{\delta\omega^2}{2} \right) \qquad [36]$$

Using the variance $\langle \omega(x)^2 \rangle$ of the local spin precession frequency

$$\langle \omega^2(x) \rangle := \frac{1}{V} \int_V dx \, \omega^2(x) = RBV \cdot \frac{\delta\omega^2}{2} \qquad [37]$$

Equation [36] can be written as

$$R_2^* = \tau \cdot \langle \omega^2(x) \rangle \qquad [38]$$

Equation [36] is just the well-known general result for transverse relaxation rate obtained for the motional narrowing limit, i.e., our result correctly describes this.

Approximation for a Small Intracapillary Volume

In many tissues, the relative fraction of intracapillary volume satisfies the condition RBV ≪ 1. Typical correla-

tion times in myocardium (and also in other tissues) are smaller than 6 ms (Eq. [11]). When considering the BOLD effect, characteristic equatorial radial frequencies $\delta\omega$ are (see Eq. [3], $\Delta\chi = 8 \cdot 10^{-8}$ (18)) for imaging systems $B_0 \leq$ 2T, lower than 270 rad s^{-1}, i.e., the condition

$$(\tau\delta\omega \cdot RBV)^2 \ll 1 \qquad [39]$$

holds. Hence, Eq. [35] leads to

$$R_2^* = RBV \cdot \tau^{-1} \cdot \left(\sqrt{1 + (\tau\delta\omega)^2} - 1 \right) \qquad [40]$$

Comparison with Simulations of Kennan et al.

Kennan et al. (10) performed Monte Carlo simulations of diffusing spins within a square box the length of which was assumed to be the distance between two neighboring capillaries. The cross-section of a capillary filled with a paramagnetic agent was located in the center of the box and the field around the capillary was that of Eq. [2]. Additionally, the fields of the four nearest neighbor capillaries were considered. These authors investigated the effect of the diffusion, intracapillary magnetization, and capillary diameter on the transverse relaxation rate for spin-echo and gradient echo experiments. Our analysis will only focus on the results of the latter.

R_2^* versus Diffusion Coefficient

For a realistic set of tissue parameters the dependence of relaxation rate on diffusion evaluated by simulation is shown in Fig. 2. It is evident that the curve determined from our model (Eqs. [11] and [35]) is similar to that
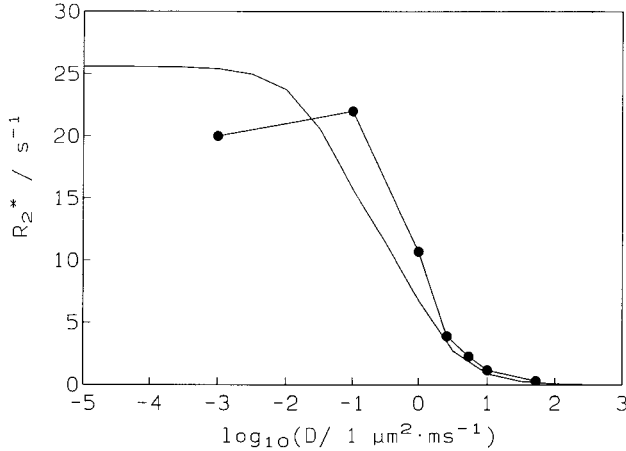
FIG. 2. Transverse relaxation rate R_2^* as a function of the tissue diffusion coefficient D. The circles denote data that were obtained by the computer simulation of Kennan et al. and taken from ref. (10) (see text). These authors assumed a capillary diameter of 5 μm and a volume fraction (RBV) of 5%. The difference of intracapillary extracapillary magnetization was chosen to be $\Delta M = \Delta\chi \cdot B_0 = 1.6$ mgauss, which would be present for deoxygenated blood ($\Delta\chi = 8 \cdot 10^{-8}$ for hematocrit = 40%) at $B_0 = 2$ T. The second curve denotes data obtained for these parameters from our model according to Eqs. [11] and [35]. The characteristic frequency and the dipole field are determined according to Eqs. [2] and [3] for $\Delta M = 1.6$ mgauss. Realistic diffusion coefficients in tissue are in the range of 1 μm²/ms, i.e., $\log_{10}(D/1 \mu m^2/ms) \approx 0$.

determined from the data points of the simulation. For smaller diffusion coefficients there is a difference of ≤20% from our model curve. It has to be stated that our model was developed under the assumption that the correlation time of field fluctuations which are induced by diffusion is considerably smaller than the BOLD-related relaxation time of magnetization. This is obviously not the case for a slow diffusion regime, i.e., small diffusion coefficients. On the other hand, Fig. 2 demonstrates that the predictions of the model are also valid for this range of diffusion coefficients. However, one has to keep in mind that in the *strong collision* model the diffusion operator $D\nabla^2$ in the time evolution operator is replaced by the operator τ^{-1} (**II** − **id**) (Eq. [23]). Both operators vanish when the diffusion coefficient approaches zero. Hence, both dynamics of field fluctuations have the same asymptotic time evolution of magnetization, which is that of the *static dephasing* regime. This explains the similarity of the model curve and the curve obtained from simulation data in the range of small diffusion coefficients.

R_2^* versus Intracapillary Magnetization

From their simulations Kennan et al. observed a power law for the dependence of relaxation rate on intracapillary magnetization, or more precisely, on the intracapillary extracapillary magnetization difference ΔM

$$R_2^* \sim \Delta M^\Lambda \qquad [41]$$

For a slow ($D = 10^{-3}$ μm²/ms), intermediate ($D = 0.65$ μm²/ms), and rapid ($D = 2$ μm²/ms) diffusion regime they obtained $\Lambda = 1.1, 1.49,$ and 1.95 respectively, when ΔM is varied from 0.1 to 1.6 mgauss. The intracapillary volume fraction was chosen for the three regimes to be RBV = 5%, 3%, and 5% and the capillary radius $R_c = 2.5$ μm in all regimes. When considered in our model, this implies correlation times of $\tau = 4930, 8.69,$ and 2.46 ms (Eq. [11]). The range of the characteristic frequency $\delta\omega$ was given by that of ΔM (Eq. [3]), i.e., it is 16.8–269 rad · s^{-1}. For the slow diffusion regime, this implies that $\tau\delta\omega \gg 1$ and Eq. [35] can be approximated by

$$R_2^* = RBV \cdot 2\delta\omega \qquad [42]$$

Since $\delta\omega \sim \Delta M$ we obtain an exponent $\Lambda = 1$ in the power law Eq. [41].

For the rapid diffusion regime, the relation $\tau\delta\omega \ll 1$ holds for the lower values of the $\delta\omega(\Delta M)$-range, i.e., according to Eq. [36] we would obtain an exponent $\Lambda = 2$. For the higher values of the characteristic frequencies the relation $\tau\delta\omega \leq 0.66$ holds, i.e., when expanding Eq. [35] in a power series of $\tau\delta\omega$, one has to consider the term of the 4th order in this variable, i.e., when RBV is small

$$R_2^* = \tau^{-1} \cdot RBV \, \tfrac{1}{2} \cdot ((\tau\delta\omega)^2 - \tfrac{1}{4} (\tau\delta\omega)^4) \qquad [43]$$

This correction explains why Kennan et al. found an exponent somewhat smaller than 2.

For the intermediate diffusion regime, we analyzed Eq. [35] for the parameters given by Kennan et al. for a magnetization range of $\Delta M = 0.16$–5 mgauss and per-

formed a linear regression analysis of this data (Fig. 3). The exponent fitted was $\Lambda = 1.61$, which is close to the value of 1.49 obtained from simulation experiments.

R_2^* versus Intracapillary Blood Volume

The authors [10] investigated the dependence of the transverse relaxation rate on the intracapillary volume fraction RBV = R_c^2/R_s^2 where they varied this parameter by increasing the capillary radius R_c or the intracapillary distance 2 R_s. In both cases, they found a nearly linear dependence; however, the slope in the case of variable intercapillary spacing was significantly smaller. We performed the same analysis. Similar to Kennan et al., we considered the diffusion coefficient $D = 0.65$ μm^2/ms and the intracapillary magnetization as 1.6 mgauss. Since Kennan et al. did not give the capillary radius and the relative intracapillary volume from where they started varying either the capillary radius or the intercapillary distance, we were not able to reproduce their simulations exactly. We determined the relaxation rate for a relative intracapillary volume of RBV = 5% and a capillary radius of 2.5 μm according to Eqs. [11] and [35]. Then we varied R_c or R_s. As in the simulations of Kennan et al., in both cases a nearly linear dependence was evident (Fig. 4), and the slope of the regression line was significantly higher in the case of a variable capillary radius $m = 2.41$ s^{-1}/% vs. $m = 1.51$ s^{-1}/%.

Comparison with Experimental Data of Atalay et al.

Atalay et al. (2) performed T_2^* sensitive gradient echo imaging at 4.7 T in the isolated red cell perfused rabbit heart at various oxygenation levels of the perfusate. This perfusate contained a cardioplegic potassium concentration to minimize oxygen utilization. Additionally the perfusate contained adenosine to achieve maximal vasodi-
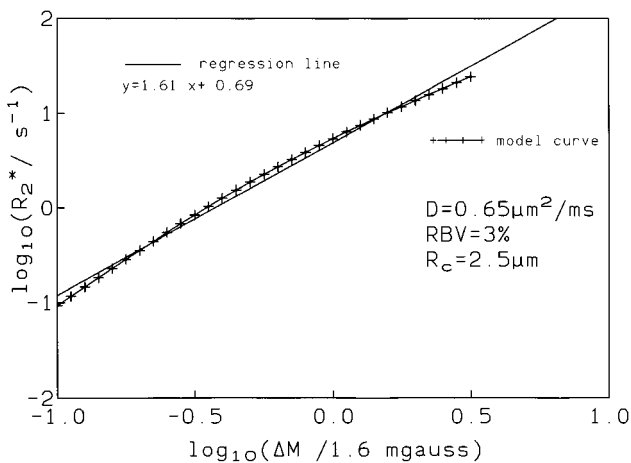
FIG. 3. Logarithm of the transverse relaxation rate as a function of the logarithm of the intracapillary extracapillary magnetization difference ΔM according to Eqs. [3] and [35]. The intracapillary volume fraction was RBV = 3%, the capillary radius was R_c = 2.5 μm, and the diffusion coefficient was D = 0.65 μm^2/ms, which were the parameters of Kennan et al. in their simulation experiments for the intermediate diffusion regime. A linear regression analysis is performed. The slope of the regression line determines the exponent of the power law (see Eq. [41] and text).
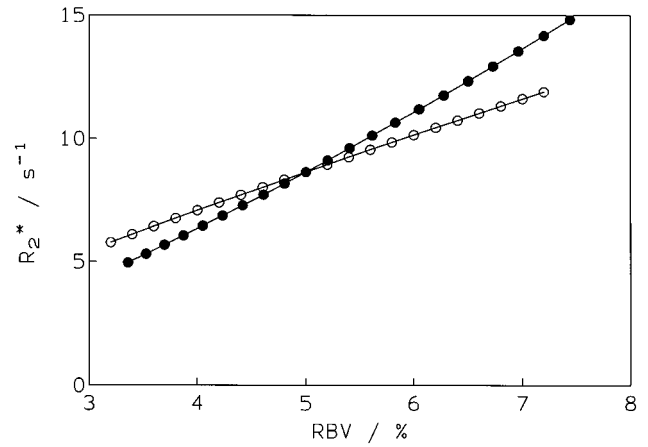
FIG. 4. Transverse relaxation rate R_2^* as a function of the relative intracapillary volume RBV obtained from Eqs. [11] and [35]. The filled circles denote data in which RBV was altered by varying the capillary radius, the open circles denote data in which the capillary radius was held constant at 2.5 μm and the intercapillary distance was varied. The diffusion coefficient was D = 0.65 μm^2/ms. The starting point of both curves was an RBV = 5% and an intracapillary radius of R_c = 2.5 μm. Linear regression analysis revealed a slope of 1.53, 2.41 s^{-1}/% for the open and the filled circle curve, respectively.

lation. Together with the results presented in their second article (3), these authors found an empirical relation between the transverse relaxation rate R_2^* and the oxygen saturation of hemoglobin in the perfusate

$$R_2^* = -37 \cdot \ln\left(0.29 + 0.7 \cdot [O_2 - \text{saturation}]\right) s^{-1}$$

$$+ 33.3 \text{ s}^{-1} \quad [44]$$

According to our model, we determined R_2^* for various RBV values (5–15%) as a function of the oxygen saturation of hemoglobin (Fig. 5). We assumed a mean capillary diameter of 5.5 μm (11) (R_c = 2.75 μm) and a diffusion coefficient of 1 μm^2/ms. According to Eq. [11], this method provides correlation times between τ = 5.96 ms (RBV = 5%) and τ = 4.22 ms (RBV = 15%). When blood is completely deoxygenated, the characteristic frequency at 4.7 T is (see Eqs. [1] and [3]) $\delta\omega$ = 632 rad · s^{-1}, and, hence, $(\tau\delta\omega \cdot \text{RBV})^2 \ll 1$, i.e., the condition of Eq. [39] holds and we can approximate relaxation rate by Eq. [40].

The intracapillary oxygenation and, hence, intracapillary magnetization, which is required for the model calculations is estimated according to the following consideration. Since cardioplegic hearts were investigated, only basal oxygen consumption has to be considered, which is about $\text{MVO}_{2,\text{basal}}$ = 0.02 ml O_2/g(tissue)/min (19). The relationship between oxygen consumption, perfusion F, and arteriovenous difference of oxygen saturation ΔY is given by

$$\dot{\text{MVO}}_{2,\text{basal}} = F \cdot \Delta Y \cdot [\text{Hb}] \cdot 1.34 \text{ ml } O_2/\text{g(Hb)} \quad [45]$$

The term [Hb] denotes the concentration of hemoglobin, and the factor 1.34 ml O_2/g(Hb) is Hüfner's number. The authors did not provide data about perfusion and concentration of hemoglobin. However, they obtained a mean
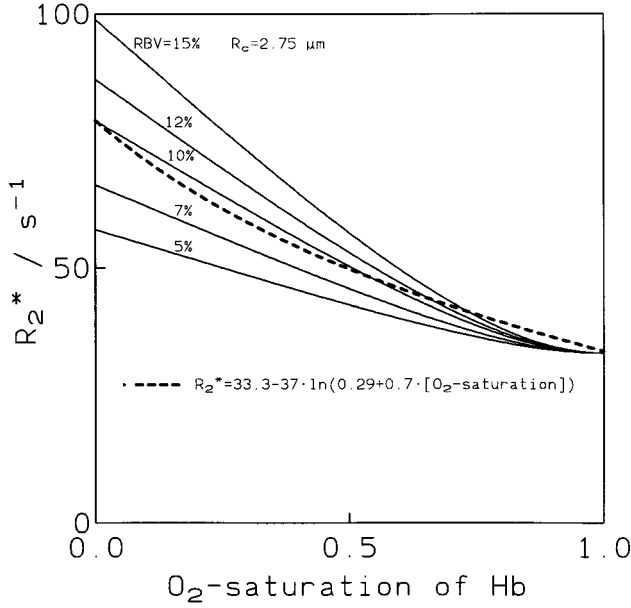
FIG. 5. Transverse relaxation rate R_2^* as a function of the oxygen saturation of hemoglobin in myocardium. The dashed curve represents the empirical curve that Atalay et al. (3) obtained from gradient echo imaging in isolated red cell perfused rabbit hearts at 4.7 T. The solid curves were obtained from our model (see Eqs. [11] and [40]), in which we assumed a capillary radius of R_c = 2.75 μm; a relative intracapillary volume of RBV = 15%, 12%, 10%, 7%, 5%; and a diffusion coefficient of D = 1 μm²/ms. Since the curves obtained from our model only considered the BOLD-related relaxation, they were given the offset of the empirical curve at 100% oxygen saturation.

coronary flow of 23 ml/min (3). Hence, a lower limit of the average perfusion can be estimated when the weight of a rabbit heart is assumed to be <15 g, i.e., F > 1.5 ml/g per min. When we assume a reasonable lower bound of hemoglobin concentration of [Hb] = 12 g/100 ml (blood), we obtain that the arteriovenous difference of oxygen saturation is

$$\Delta Y < 8.3\% \qquad [46]$$

which is considerably smaller than the arteriovenous difference of a beating heart ($\approx 70\%$). This finding suggests that the gradient of the intracapillary oxygen saturation may be neglected, i.e., the intracapillary oxygenation level is almost that of the perfusate Y_p. Thus, we determined $\delta\omega$ according to Eqs. [1] and [3] for the susceptibility difference $\Delta\chi = (1 - Y_p) \cdot \Delta\chi_0$, with $\Delta\chi_0 = 8 \cdot 10^{-8}$ as the susceptibility difference for complete deoxygenated blood. Since experiments were performed in a horizontal system, the long heart axis, and, hence, the mean orientation of the capillaries was most probably perpendicular to the direction of the external field, i.e., the assumption that $\theta = \pi/2$ (Eqs. [1] and [3]) is reasonable, and the equatorial shift of the radial frequency is $\delta\omega = 2\pi\gamma \cdot (1 - Y_p)\Delta\chi_0 \cdot B_0$.

Since we can only determine the BOLD-related part of relaxation, the offset of the empirical function (Eq. [44]) at 100% oxygen saturation of hemoglobin ($R_2^*(O_2$ sat. = 1) = 33.3 s⁻¹) was added to our data. Figure 5 demonstrates clearly similarity between the empirical curve and the

curve obtained from our model when RBV = 10%, which is a reasonable value for a dilated microvascular system (20).

Comparison with Our Own Results

We performed diastolic measurements of myocardial T_2^* in healthy volunteers (n = 15) in the short axis view by a segmented gradient echo sequence, which acquires 10 successive gradient echoes per excitation (TE = 6–54 ms, ΔTE = 5.4 ms). The exact description of the method, the protocol, and the results is given in detail in another article (C. Wacker, et al., manuscript submitted). In this section, only the essentials of the results are reported to demonstrate that the theory may be applied in this field. Measurements were performed before and after application of the vasodilator dipyridamol (0.56–0.84 mg/kg body weight, continuous infusion) in a 1.5 T system. In this dosage, dipyridamol has the property to increase coronary blood flow from a value at rest of $F_{rest} \approx 0.8$ ml/g per min to $F_{dipyridamol}$ = 4 ml/g per min (21) with negligible effect on myocardial performance, and hence, oxygen consumption. Thus, the capillary deoxyhemoglobin concentration should decrease and the BOLD effect should become evident. The mean T_2^* we determined under resting conditions was 36 ms, and we observed an increase of about 17% after dipyridamol administration.

Under resting conditions, the oxygen pressure in the venous coronary system is about 17 Torr (22), i.e., the oxygenation of hemoglobin is about $Y_{v,rest}$ = 25%. Arterial oxygenation is almost $Y_a \approx 100\%$, and the myocardial oxygen consumption $\dot{MVO_2}$ is proportional to coronary blood flow and the arteriovenous difference of oxygenation $\Delta Y_{rest} = Y_a - Y_{v,rest}$, i.e.

$$\dot{MVO_2} \sim F \cdot \Delta Y \qquad [47]$$

Since dipyridamol does not alter the oxygen consumption $\dot{MVO_2}$, administration of this drug reduces the arteriovenous difference to

$$\Delta Y_{dipyridamol} = \frac{F_{rest}}{F_{dipyridamol}} \cdot \Delta Y_{rest} \qquad [48]$$

$$= 15\%, \qquad [49]$$

i.e., the venous oxygenation after dipyridamol administration is $Y_{v,dipyridamol} \approx 85\%$.

As a first step to estimate the myocardial BOLD effect according to our model, we consider the intracapillary oxygenation to be Y_v. The dependence of the susceptibility difference $\Delta\chi$ on oxygenation is determined by $\Delta\chi = \Delta\chi_0 \cdot (1 - Y_v)$, with $\Delta\chi_0 = 8 \cdot 10^{-8}$ for deoxygenated blood with a hematocrit of 40%. When we take a capillary radius of 2.75 μm, an intercapillary distance of 19 μm (11), and a diffusion coefficient of D = 1 μm²/ms, the intracapillary volume fraction is RBV = 8.4% and the correlation time τ = 5.11 ms (Eq. [11]). Insertion into Eqs. [1]–[3], and [35] gives a BOLD-related relaxation rate of R_2^* = 4.43 s⁻¹ under resting conditions and R_2^* = 0.2 s⁻¹ after dipyridamol application. Hence, the BOLD-related decrease of relaxation rate is ΔR_2^* = −4.23 s⁻¹. Under resting conditions, we measured a mean $T_{2,rest}^* \approx 36$ ms, i.e., $R_{2,rest}^*$ = 27.7 s⁻¹.

Thus, our calculations would predict a rate of $R^*_{2,\text{dipyridamol}} = 23.47$ s^{-1} after dipyridamol administration, i.e., $T^*_{2,\text{dipyridamol}} = 42.6$ ms. Similar calculations reveal for capillary oxygenation levels of Y = 30%, 35%, 40%, and 50% corresponding relaxation times of $T^*_{2,\text{dipridamol}} = 41.6$ ms, 40.8 ms, 40 ms, and 39 ms, respectively. Hence, calculations performed for a capillary oxygenation at rest in the range of 25–35% predict an increase of $T^*_{2,\text{rest}}$ by 13–18%, which is in good agreement with the increase of 17% obtained from experimental data.

It has to be stated that the considerations above are rather crude. For example, we did not consider an intracapillary gradient of oxygenation along the capillary axis. However, the determination of such a gradient in myocardium is very difficult. In the brain, for example, almost stationary conditions of perfusion and oxygen consumption suggest a stationary gradient of oxygenation in the direction of the capillary axis. In the beating heart, the contractions of myocardium lead to cyclic variations of oxygen consumption and intracapillary flow. Thus, the intracapillary oxygenation is a complex function of the phasic oxygen demand, phasic intracapillary red cell flux, and the diffusion controlled oxygen transport from hemoglobin to extracapillary tissue. Some theories (23) assume a rapid delivery of oxygen from all intracapillary red blood cells in early diastole, i.e., intracapillary oxygenation would rapidly decrease to that of the venous system in early diastole. This hypothesis would be in accordance with our calculations that predict the observed increase of T^*_2 best when the intracapillary oxygenation is close to that of the coronary venous system. However, other theories assume several heart cycles for the delivery of oxygen, which suggests the formation of a longitudinal gradient of intracapillary oxygenation (23). To our knowledge no experimental data exist of these gradients of intracapillary oxygenation in myocardium. Hence, we think that our assumption above is justified as a first step to estimate the BOLD effect in myocardium.

DISCUSSION

Based on a simple model geometry of capillary and surrounding tissue we derived an analytical expression for the transverse relaxation rate as a function of the relative capillary volume fraction, the capillary radius, the intracapillary magnetization and the diffusion coefficient. The decisive step that allowed this analytical approach was the application of the *strong collision* approach to the dynamics of spin diffusion. The predictions of the model agree well with the data obtained by simulation experiments of Kennan et al. (10) and the experimental results of Atalay et al. (2, 3) and our group (C. Wacker, et al., manuscript submitted). It has to be emphasized that our approach may also be transferred to other capillary arrangements besides that in myocardium.

Model Assumptions

We considered diffusion between coaxial cylinders, i.e., the capillary and the supply cylinder. One might argue, that we did not consider a rectangular geometry for the diffusion space as others did for their simulations (10).

However, for morphometric analysis in myocardium a hexagonal arrangement of capillaries is often assumed (11, 24). The capillary supply distance (half of the mean intercapillary distance) is $R_s = 1/\sqrt{\text{capillary density} \cdot c}$ with $c = 2\sqrt{3} = 3.46$ for the hexagonal, $c = \pi$ for the cylindrical, and $c = 4$ for the rectangular model, i.e., the cylindrical model is closer to the hexagonal one than the rectangular. Furthermore, mathematical analysis is performed much easier in the cylindrical model, and the intention of our article preferred to demonstrate fundamental properties of our model rather than to reproduce morphometrical exactness.

Within the diffusion space, we only considered the interaction of a nuclear spin with the magnetic field around one capillary, i.e., **the field contribution of the neighboring capillary** was neglected. In myocardium, the intercapillary distance is about 19 μm and the capillary radius 2.75 μm (11). Hence, the contribution of a neighboring field at the periphery of the supply region field is less than 10% from its maximum, i.e., as a first step it is justified to neglect these fields.

In our model, we did not consider intravascular contributions to the BOLD effect. Boxerman et al. (25) performed Monte Carlo simulations of diffusing spins to quantitate signal changes in fMRI. The physiological and anatomical parameters they applied in their simulations were that of the brain. For an echo time of TE = 40 ms and a relative flow increase of e.g. 1.6, they obtained a BOLD-related signal change of $\approx$1%, which is related to the extravascular magnetization, and $\approx$2% when the intracapillary and extravascular components are considered. When all components that contribute to the BOLD effect are considered, i.e., extravascular, intracapillary, and intravenous magnetization, the signal change was about 3.5%. Hence, the authors state that the intravascular contribution of the BOLD effect to signal change is clearly dominating. In our model, we did not consider the intravascular or intracapillary contribution to the BOLD effect, since the anatomical and physiological situation is different in myocardium. In myocardium the intravascular volume consists mainly of the intracapillary volume (>90%) (7), whereas the volume of the venous system is less than 10% of the intravascular volume. In the brain, however, the volume fractions of both the intracapillary and intravenous system are almost the same (25). This finding suggests that the contribution of the venous system to the BOLD effect is considerable in the brain, although it may be negligible in myocardium. When we restrict our considerations to the capillary system, there are also decisive differences between both tissues: the relative volume fraction of the intracapillary space is higher in myocardium ($\approx$8.4% (12)) than in the brain ($\approx$2%), which implies that more extravascular spins are affected by the pericapillary magnetic field gradient in myocardium than in the brain. Another point is that the oxygen extraction within the capillary is much higher in myocardium. This finding leads to a venous oxygenation of about 25%, whereas in the brain it is 60%. Furthermore, there is phasic oxygen delivery in myocardium, i.e., there is not stationary oxygenation gradient along the capillary axis as there is in the brain. Some authors even assume that almost the whole oxygen delivery takes place in early diastole (23), i.e., the intracapillary oxygenation would

rapidly decline to that of the coronary venous system during diastole. This finding suggests that the magnitude of the pericapillary magnetic field, and hence, the contribution of the extravascular relaxation enhancement to the BOLD effect is much higher in myocardium than in the brain. This finding can also be quantified as follows: a relative signal change of about 1% (TE = 40 ms) due to the extravascular contribution of the BOLD effect in the brain (25) suggests an increase of the relaxation rate of $\Delta R_2^* = 0.25 \text{ s}^{-1}$, when we assume that the relative signal change is $1 - e^{-\text{TE} \cdot \Delta R_2^*} \approx \text{TE} \cdot \Delta R_2^*$. In myocardium, our model, which only considers extravascular BOLD effects, reveals reasonable increases of relaxation rate in the order of $\Delta R_2^* \approx 4 \text{ s}^{-1}$, i.e., 16 times higher than that in the brain. Therefore, we think that as a first step it is justified to consider only the extravascular magnetization and its contribution to relaxation in myocardium. Nevertheless, our model may be developed to a model that also includes the effect of intracapillary magnetization. In this case, tissue is considered as a two-compartment system, with two intrinsic relaxation rates: the intracapillary and the extravascular relaxation rate, of which the latter is determined according to our model. In another context, we recently derived an analytical expression that provides the relaxation rate of such a two-compartment system as a function of the intracapillary and extravascular relaxation rate, and the exchange rate between both compartments (26). The application of this complex model will be one of our future aims.

In our model, capillaries are considered as cylinders filled with blood. Blood inside the capillaries is assumed to be a homogeneous magnetic substance, and the pericapillary magnetic field is determined according to principles of magnetostatics. This assumption is valid in larger vessels; however, in capillaries the situation is different. The cross-section of a capillary is approximately the size of an erythrocyte. This finding suggests that blood inside the capillary may be considered as an almost linear arrangement of single red blood cells with plasma in between. The BOLD effect is related to the paramagnetic property of deoxyhemoglobin, which is confined to the red blood cells. Thus, the inhomogeneous magnetic field in tissue is a superposition of the magnetic fields around the red blood cells. This finding suggests that the pericapillary field strength is stronger in the near side of capillary segments that contain an erythrocyte than in segments in between that are filled with plasma. This pericapillary magnetic field is obviously more complex than the field around a homogeneous paramagnetic cylinder, as we assumed in our model. However, the determination of this complex field is hampered by several obstacles: the toroidal shape of red blood cells in large vessels changes as these cells enter the capillary, due to mechanical and hydrodynamical interactions of the erythrocyte with the capillary wall and plasma. There is no simple mathematical description for this intracapillary shape of red blood cells, i.e., the magnetic field outside the cell cannot be described by a simple formula. Furthermore, this intracapillary shape of the erythrocyte may be a time-dependent function of mechanical forces, e.g., intramural cyclic pressure variations in myocardium. Due to this complicated situation, it appears that at the present state of knowledge our capillary-tissue model may be a reasonable approach to start with. This model bears the potential to be elaborated for a more realistic, and, hence, complex description of structures in tissue.

Relaxation

We assumed in our analysis a single exponential decay of the relaxation curve. One might argue that in general a multiexponential fit has to be applied. However, at present, the experimental data do only reveal enough information to justify a single exponential approach. Furthermore, our model is not limited to a single exponential fit, but it can be expanded to a multiexponential fit of any order. Since we could determine the Laplace transform (Eq. [30]) of the transverse magnetization decay, the full information of the exact relaxation curve is available. Based on the theory of generalized moment expansion, one of us recently developed an algorithm that allowed a multiexponential approximation of nth order of the relaxation curve from the Laplace transform (15). We had already applied this multiexponential approximation to spin relaxation (17); however, we believe experimental data suggesting a non-single exponential decay should be a prerequisite.

In our study, we only considered the decay of magnetization that is detected by gradient echo sequences, i.e., reversible and irreversible dephasing effects contribute to transverse relaxation. In contrast, in spin-echo sequences, irreversible dephasing effects are detected. In principle, time evolution of magnetization in spin-echo sequences may also be determined according to the *strong collision* model. The operator of time evolution in Eq. [23] has to be replaced by a sequence of this operator and its complex adjoint operator, in which the latter describes the time evolution after the 180° pulse. When multiecho sequences with n echoes is used, this operator sequence has to be repeated n times. Obviously, the mathematical analysis of this relaxation is much more complex and will be one of our future goals.

APPENDIX

Derivation of the Correlation Time

The solution of Eq. [11] requires the determination of a function $f(x) = -(1/\nabla^2)\omega(x)$. This function has to satisfy the inhomogeneous differential equation

$$\nabla^2 f(x) = -\omega(x) \qquad [\text{A1}]$$

Since $\omega(x) = -\delta\omega \cdot R_c^2 \cdot \cos(2\phi)/r^2$ (cylindrical coordinates $x = (r, \phi)$), we make the approach

$$f(x) = g(r) \cdot \cos(2\phi) \qquad [\text{A2}]$$

Application of the operator $\nabla^2 = r^{-1}\partial_r r\partial_r + r^{-2}\partial_\phi^2$ (cylindrical coordinates) on f results in

$$\partial_r^2 g(r) + r^{-1}\partial_r g(r) - 4r^{-2}g(r) = \delta\omega R_c^2 r^{-2} \qquad [\text{A3}]$$

Equation [A3] is solved by

$$g(r) = a \cdot r^2 + b \cdot r^{-2} - \frac{\delta\omega \cdot R_c^2}{4} \qquad [A4]$$

where the constants a and b are determined so that Eq. [A4] satisfies the boundary conditions of the diffusion process, i.e., $\partial_r g(r) = 0$ when $r = R_c, R_s$. This implies that $a = b = 0$, i.e.,

$$f(x) = -\cos(2\phi) \cdot \frac{\delta\omega R_c^2}{4} \qquad [A5]$$

Insertion of f in Eq. [11] gives

$$\tau = \frac{1}{K(0)DV} \cdot \int_V dx\, \omega(x) \cdot f(x) \qquad [A6]$$

$$= \frac{1}{K(0)V} \cdot \int_{R_c}^{R_s} \int_0^{2\pi} dr\, r d\phi\, \cos^2(2\phi) r^{-2} \cdot \frac{\delta\omega^2 R_c^4}{4D} \qquad [A7]$$

$$= \frac{1}{K(0)V} \cdot \ln(R_s/R_c) \frac{\pi\delta\omega^2 R_c^4}{4D} \qquad [A8]$$

with

$$K(0) = \frac{1}{V} \int_V dx\, \omega(x)^2 \qquad [A9]$$

$$= \frac{1}{V} \int_{R_c}^{R_s} \int_0^{2\pi} dr\, r d\phi (\delta\omega R_c^2 \cdot \cos(2\phi) r^{-2})^2 \qquad [A10]$$

$$= \frac{1}{V}(R_c^{-2} - R_s^{-2}) \frac{\pi\delta\omega^2 R_c^4}{2} \qquad [A11]$$

this directly provides the result of Eq. [11].

Derivation of the Laplace transform $\hat{M}_0(s)$

The Laplace transform of the time course of magnetization in the absence of diffusion (static dephasing regime) is

$$\hat{M}_0(s) = \frac{1}{V} \int_V dx \frac{1}{s \cdot \mathbf{id} - i \cdot \omega(x)}$$

$$= \frac{1}{V} \int_{R_c}^{R_s} dr \cdot r \int_0^{2\pi} d\phi \cdot \frac{1}{s \cdot \mathbf{id} - i \cdot (-\delta\omega \cdot R_c^2 \cos(2\phi)/r^2)}$$

$$= \frac{1}{V} \int_{R_c}^{R_s} dr\, r^3 \underbrace{\int_0^{2\pi} d\phi \frac{1}{r^2 s + i\delta\omega R_c^2 \cos 2\phi}}_{= I(r)} \qquad [A12]$$

Elementary integral transformation and substitution of $e^{i\phi} = z$ provides the integral $I(r)$

$$I(r) = \int_0^{2\pi} d\phi \frac{1}{r^2 s + i\delta\omega R_c^2 \cos 2\phi}$$

$$= \int_0^{2\pi} d\phi \frac{1}{r^2 s + i\delta\omega R_c^2 \cos \phi}$$

$$= \oint_{|z|=1} dz \frac{1}{iz} \cdot \frac{1}{r^2 s + i\delta\omega R_c^2 \frac{1}{2}\left(z + \frac{1}{z}\right)}$$

$$= -\oint_{|z|=1} dz \frac{1}{R_c^2 \delta\omega^{1/2}(z^2 + 1) - isr^2 z}$$

$$= -2\pi i \cdot \mathrm{Res}\left(\frac{1}{R_c^2 \delta\omega^{1/2}(z^2 + 1) - isr^2 z}, |z_p| < 1\right)$$

$$= -2\pi i \cdot \frac{1}{R_c^2 \delta\omega/2} \cdot \frac{1}{z_{p1} - z_{p2}}$$

$$= 2\pi \frac{1}{\sqrt{s^2 r^4 + R_c^4 \delta\omega^2}} \qquad [A13]$$

where $z_{p2} = i \cdot [sr^2 + \sqrt{(s^2 r^4 + R_c^4\delta\omega^2)}/(R_c^2\delta\omega)]$ and $z_{p1} = i \cdot [sr^2 - \sqrt{(s^2 r^4 + R_c^4\delta\omega^2)}/(R_c^2\delta\omega)]$ denote the poles of the complex function $(R_c^2\delta\omega^{(1/2)}(z^2 + 1) - isr^2 z)^{-1}$. The absolute value of the latter is smaller than 1.

Substitution of the right-hand side of Eq. [A13] in Eq. [A12] provides

$$\hat{M}_0(s) = \frac{2\pi}{V} \int_{R_c}^{R_s} dr\, r^3 \frac{1}{\sqrt{s^2 r^4 + R_c^4\delta\omega^2}}$$

$$= \frac{2\pi}{4Vs^2} \int_{s^2 R_c^4}^{s^2 R_s^4} d\xi \frac{1}{\sqrt{\xi + R_c^4\delta\omega^2}} = \frac{1}{s^2 \cdot (R_s^2 - R_c^2)}$$

$$\cdot \left(\sqrt{s^2 R_s^4 + \delta\omega^2 R_c^4} - R_c^2\sqrt{s^2 + \delta\omega^2}\right)$$

$$= \frac{R_c^2 + R_s^2}{\sqrt{s^2 R_s^4 + \delta\omega^2 R_c^4} + R_c^2\sqrt{s^2 + \delta\omega^2}} \qquad [A14]$$

REFERENCES

1. Ogawa S, Lee T-M, Nayak AS, Glynn P. Oxygenation-sensitive contrast in magnetic resonance image of the rodent brain at high magnetic fields. Magn Reson Med 1990; 14:68–78.
2. Atalay MK, Forder JR, Chacko VP, Kawamoto S, Zerhouni EA. Oxygenation in the rabbit myocardium: assessment with susceptibility dependent MR imaging. Radiology 1993; 189:759–764.
3. Atalay MK, Reeder SB, Zerhouni EA, Forder JR. Blood oxygenation dependence of T_1 and T_2 in the isolated, perfused rabbit heart at 4.7 T Magn Reson Med 1995; 34:623–627.
4. Li D, Dhawale P, Rubin PJ, Haacke EM, Gropler RJ. Myocardial signal response to dipyridamol and dobutamine: demonstration of the BOLD effect using a double-echo sequence. Magn Reson Med 1996; 36:16–20.

5. Niemi P, Poncelet BP, Kwong KK, Weisskoff RM, Rosen BR, Brady TJ, Kantor HL. Myocardial intensity changes associated with flow stimulation in blood oxygenation sensitive magnetic resonance imaging. Magn Reson Med 1996; 38:78–82.

6. Yablonski DA, Haake EM. Theory of NMR-signal behavior in magnetically inhomogeneous tissues: the static dephasing regime. Magn Reson Med 1994; 32:749–763.

7. Kaul S, Jayaweera AR. Coronary and myocardial blood volumes. Circulation 1997; 96:719–724 [Editorial].

8. Gillis P, Koenig SH. Transverse relaxation of solvent protons induced by magnetized spheres: application to ferritin, erythrocytes, and magnetite. Magn Reson Med 1987; 5:323–345.

9. Torrey HC. Bloch equations with diffusion terms. Phys Rev 1956; 104:563–565.

10. Kennan RP, Zhong J, Gore JC. Intravascular susceptibility contrast mechanisms in tissues. Magn Reson Med 1994; 31:9–21.

11. Bassingwaighte JB, Ypintsol T, Harvey RB. Microvasculature of the dog left ventricular myocardium. Microvasc Res 1974; 7:229–249.

12. Donahue KM, Burstein D, Mannings WJ, Gray ML. Studies of Gd-DTPA relaxivity and proton exchange rates in tissue. Magn Reson Med 1994; 32:66–76.

13. Bauer WR, Schulten K. Theory of contrast agents in magnetic resonance imaging: coupling of spin relaxation and transport. Magn Reson Med 1992; 26:16–39.

14. Jackson DJ. "Classical Electrodynamics," John Wiley and Sons, New York, 1975.

15. Nadler W, Schulten K. Generalized moment expansion for Brownian relaxation processes. J Chem Phys 1985; 82:151–160.

16. Dattagupta S, Blume M. Stochastic theory of line shape: I. Nonsecular effects in the strong collision model. Phys Rev B 1974; 10:4540–4550.

17. Bauer WR, Schulten K. Nuclear spin dynamics ($I = 1/2$) under the influence of random perturbation fields in the strong collision approximation. Ber Bunsenges Phys Chem 1992; 96:721–723.

18. Thulborn KR, Waterton JC, Mathews PM, Radda G. Oxygenation dependence of the transverse relaxation time of water protons of whole blood at high fields. Biochim Biophys Acta 1982; 714:265–270.

19. Groth J, Thews G. Die Bedingungen für die Sauerstoffversorgung des Herzmuskelgewebes. Pflügers Arch 1962; 276:142–165.

20. Chrystal GJ, Downey HF, Bashour FA. Small vessel and total coronary blood volume during adenosine infusion. Am J Physiol 1981; 241:H194–H201.

21. Tauchert M, Hilger HH. in "The Pathophysiology of Myocardial Perfusion" (W. Shaper, Ed.), p. 141, Elsevier/North Holland Biomedical Press, Amsterdam, 1979.

22. Bing RJ, Hammond MM, Handelsman JC, Powers SR, Spenger FC, Eckenhoff JE, Goodale WT, Hafkenschiel JH, Kety SS. The measurement of coronary blood flow, oxygen consumption, and efficiency of the left ventricle in man. Am Heart J 1949; 38:1.

23. Thews G. Die Sauerstoffdrücke im Herzmuskelgewebe. Pflügers Arch 1962; 276:166–181.

24. Gerdes AM, Callas G, Kasten FH. Differences in regional capillary distribution and myocyte sizes in normal and hypertrophic rat hearts. Am J Anat 1979; 156:523–532.

25. Boxerman JL, Bandettini PA, Kwong KK, Baker JR, Davis TL, Rosen BR, Weisskoff RM. The intravascular contribution to fMRI signal change: Monte Carlo modeling and diffusion weighted studies in vivo. Magn Reson Med 1995; 34:4–10.

26. Bauer WR, Roder F, Hiller K-H, Han H, Fröhlich S, Rommel E, Haase A, Ertl G. The effect of perfusion on T_1 after slice-selective spin inversion in the isolated cardioplegic rat heart: measurement of a lower bound of intracapillary-extravascular water proton exchange. Magn Reson Med 1997; 38:917–923.